Formation of STM images of Ni_3Al (001) and (111) surfaces

L. Jurczyszyn
Institute of Experimental Physics, University of Wrocław, plac Maksa Borna 9, 50–204 Wrocław, Poland

A. Rosenhahn, J. Schneider, C. Becker, and K. Wandelt
Institut für Physikalische und Theoretische Chemie, Universität Bonn, Wegelerstrasse 12, D-53115 Bonn, Germany

(Received 10 July 2002; revised manuscript received 17 April 2003; published 26 September 2003)

We present the results of scanning tunnel microscope (STM) measurements performed on a $Ni_3Al(111)$ surface, combined with a theoretical study of the formation of STM images of (001) and (111) surfaces of this alloy. The STM images of the $Ni_3Al(111)$ surface show a superstructure with the lattice constant corresponding to the size of the surface unit cell. An earlier interpretation of this result assumes that this superstructure represents the distribution of the surface Al atoms, while Ni atoms remain invisible in the STM images. This supposition is confirmed here by presented STM simulations. Moreover, numerical calculations show that a similar effect should also appear in the STM images of the $Ni_3Al(001)$ surface. A detailed theoretical analysis indicates that the domination of Al atoms in the STM images of both surfaces is mainly caused by the intra-atomic s-p_z interference. This kind of intra-atomic interference reduces the s and p_z current contributions tunneling through surface Ni atoms and increases considerably the corresponding contributions flowing through Al atoms. As a result, only the surface Al atoms appear in the STM images.

DOI: 10.1103/PhysRevB.68.115425 PACS number(s): 68.37.Ef, 73.20.−r, 78.66.Bz

I. INTRODUCTION

This paper presents scanning tunnel microscope (STM) measurements performed for a (111) surface of paramagnetic Ni_3Al and also the theoretical study of the formation of STM images of (001) and (111) surfaces of this alloy.

It follows from fcc geometry that in the case of the (001) surface the topmost atomic layer may have a mixed structure with 50% Ni-50% Al composition (mixed layer) or 100% Ni composition. Nevertheless, the results received from the low-energy electron diffraction (LEED) indicate that a more stable configuration is given by the mixed layer termination.[1,2] This experimental result was also confirmed by first-principles calculations of the cohesive energy of a three-layer slab, which show that the largest energy is obtained for a slab with mixed surface termination.[1] I-V LEED measurements of $Ni_3Al(001)$ indicate also that the topmost layer of Al atoms appears to be displaced 0.02 Å outwards with respect to the Ni surface atoms.

In the case of the (111) surface of ordered Ni_3Al, all the (111) planes are equal with the stoichiometric composition of three Ni and one Al atoms. The experimental data obtained from I-V LEED measurements of the clean $Ni_3Al(111)$ surface reveals a bulklike structure, where surface Al atoms are slightly moved outwards by 0.06 Å with respect to the plane of Ni atoms.[3]

The STM images presented in Ref. 4 and in this paper (cf. Fig. 1) show a 2×2 superstructure with the same lattice constant spacing as the size of the surface unit cell. The interpretation of this result proposed in Ref. 4 considers that this superstructure represents the distribution of the surface Al atoms, while Ni atoms remain invisible in these images. In order to verify this assumption and to clarify the mechanism, which is responsible for this effect, we have performed a theoretical study of the STM process at the $Ni_3Al(111)$ surface and for comparison also for the (001) surface of the same alloy. The theoretical results received from these STM simulations have been compared with experimental data and are discussed especially in the context of the role of interorbital interference in the tunneling process and its influence on the atomic corrugations in STM images of the (001) and (111) surfaces.

II. RESULTS OF STM MEASUREMENTS

The STM measurements were performed in a UHV system equipped with a STM, a vibrating Kelvin probe, an Auger electron spectrometer with a cylindrical mirror analyzer,

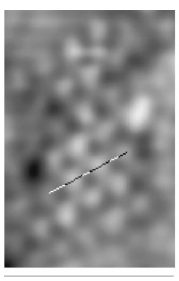

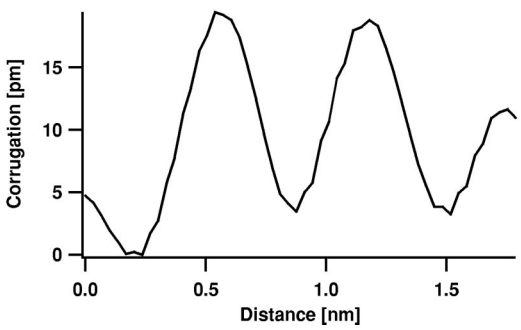

FIG. 1. Atomically resolved STM image of the $Ni_3Al(111)$ surface showing a superstructure formed by surface Al atoms and a linescan through a dense-packed row as shown. Image size, 3.5×5.3 nm^2; tunneling parameters, $U=20$ mV, $I=1.5$ nA.

and a quadrupole mass spectrometer for residual gas analysis. The concept and construction of the self-designed and built STM has been described in greater detail elsewhere.[5,6] The base pressure of the UHV system was less than 3×10^{-10} mbars.

The $Ni_3Al(111)$ single crystal was oriented with 0.5° accuracy and mechanically polished by MaTeck in Jülich. Once in UHV, the sample was cleaned by Ar-ion sputtering (2.5 keV, 2.6 $\mu A/cm^2$) at 600 K. In order to smooth the surface, the sample was annealed for 5 min at 1150 K and for 5 min at 1000 K. Sputtering and annealing cycles were repeated until the Auger spectra and STM images showed a clean and ordered surface.

Figure 1 shows an atomically resolved STM image of the clean (111) surface of Ni_3Al. As reported earlier (cf. Ref. 4), the images show hexagonal arrangements with a lattice constant of about 5.074 Å. This distance corresponds well with the (2×2) superstructure of the unit cell of the surface due to the ordered distribution of Al and Ni atoms.[3] The nearest Ni-Ni distance at the surface is 2.537 Å and cannot be seen in the STM images. As the linescan in Fig. 1 is slightly off the *x*-scan direction, it reveals a small drift resulting in a distance between two maxima which is slightly larger than the expected 5.074 Å. The corrugation of the observed atomic features is about 15 pm and changes with the tip condition. The given value represents the upper limit of what has been found in the measurements. The bias voltage in this experiment was $+20$ mV, and at this point it is important to stress that the experimental setup requires this voltage to be applied to the sample. This means that at the given voltage tunneling occurs from the tip into the unoccupied states of the sample.

III. METHOD OF CALCULATION

The calculations of the STM tunneling current presented in this paper are based on the nonequilibrium Green-function formalism, developed by Keldysh.[7] This method was used by Carolli *et al.* in theoretical studies of electronic tunneling in microstructures,[8,9] and later it was also adopted in the theory of STM.[10,11] In this approach, the tunneling process is represented by the coherent superposition of the tunneling through different channels formed by orbitals of the tip and the sample.

The complete Hamiltonian of the whole tip-sample system can be written as a sum of three terms, describing the tip ($\hat{H}_T$), sample ($\hat{H}_S$), and the interaction between them ($\hat{H}_I$):

$$\hat{H}=\hat{H}_T+\hat{H}_S+\hat{H}_I, \tag{1}$$

where the tip-sample interaction can be expressed as a result of the hopping processes between the orbitals of the tip and sample atoms:

$$\hat{H}_I=\sum_{\alpha,j}\left[\hat{T}_{TS}(\alpha j)\hat{c}_T^{\dagger}(\alpha)\hat{c}_S(j)+\hat{T}_{ST}(j\alpha)\hat{c}_S^{\dagger}(j)\hat{c}_T(\alpha)\right]. \tag{2}$$

Summation in Eq. (2) is performed over the orbitals from both parts of the system. The elements of the matrix $\hat{T}_{TS}$ denote hoppings between the orbitals of the tip and the sample. When the tip-sample system is in a stationary state (determined by the applied voltage), the total tunneling current between the tip and the sample can be written as follows:[9]

$$J=(ie/\hbar)\sum_{\alpha,j}\left[\hat{T}_{TS}(\alpha j)\langle\hat{c}_T^{\dagger}(\alpha)\hat{c}_S(j)\rangle - \hat{T}_{ST}(j\alpha)\langle\hat{c}_S^{\dagger}(j)\hat{c}_T(\alpha)\rangle\right]. \tag{3}$$

As it has been shown in previous papers,[12] the Keldysh formalism allows us to pass from a general formula (3) to the following equation for the tunneling current:

$$J=(4\pi e/\hbar)\int_{-\infty}^{+\infty}\mathrm{Tr}[\hat{T}_{TS}\hat{\rho}_{SS}(\omega)\hat{D}_{SS}^{R}(\omega)\hat{T}_{ST}\hat{\rho}_{TT}(\omega)\hat{D}_{TT}^{A}(\omega)] \times[f_T(\omega)-f_S(\omega)]d\omega, \tag{4}$$

where

$$\hat{D}_{SS}^{R}(\omega)=[\hat{I}-\hat{T}_{ST}\hat{g}_{TT}^{R}(\omega)\hat{T}_{TS}\hat{g}_{SS}^{R}(\omega)]^{-1} \tag{5}$$

and

$$\hat{D}_{TT}^{A}(\omega)=[\hat{I}-\hat{T}_{TS}\hat{g}_{SS}^{A}(\omega)\hat{T}_{ST}\hat{g}_{TT}^{A}(\omega)]^{-1}. \tag{6}$$

Equation (4) shows that for the calculation of the tunneling current we need to know the matrices of the Green functions ($\hat{g}_{TT}^{A}$ and $\hat{g}_{TT}^{R}$ for the tip; $\hat{g}_{SS}^{A}$ and $\hat{g}_{SS}^{R}$ for the sample) and the density of states ($\hat{\rho}_{TT}$ for the tip; $\hat{\rho}_{SS}$ for the sample) when the tip and the sample are uncoupled (i.e., when $\hat{T}_{TS}=0$). We also have to find the matrix $\hat{T}_{TS}$ for hoppings between the orbitals from the tip and the sample; it has been demonstrated in Ref. 13 that these hopping interactions can be calculated using the Bardeen tunneling current between the atomic orbitals ψ_i and ψ_j multiplied by coefficient γ:

$$T_{i,j}=-(\gamma/2)\int_{\rho_{i,j}}dS(\psi_i\nabla\psi_j-\psi_j\nabla\psi_i), \tag{7}$$

where γ typically takes values between 1.3 and 1.5 (for more details see Ref. 13).

The calculation of the electronic structure of the Ni_3Al surfaces has been performed with the help of the self-consistent (LCAO) linear combination of atomic orbitals method, described in more detail previously.[14,15] In this approach, the LCAO Hamiltonian is constructed as a sum of two following terms:

$$\hat{H}=\hat{H}^{oe}+\hat{H}^{mb}, \tag{8}$$

where $\hat{H}^{oe}$ defines the one-electron contribution

$$\hat{H}^{oe}=\sum_{i,\delta}E_{i\delta}\hat{n}_{i\delta}+\sum_{\delta,(i,j)}\hat{T}_{i,j}^{\delta}(\hat{c}_{i,\delta}^{\dagger}\hat{c}_{j,\delta}+\hat{c}_{j,\delta}^{\dagger}\hat{c}_{i,\delta}), \tag{9}$$

while $\hat{H}^{mb}$ corresponds to the many-body part of the Hamiltonian

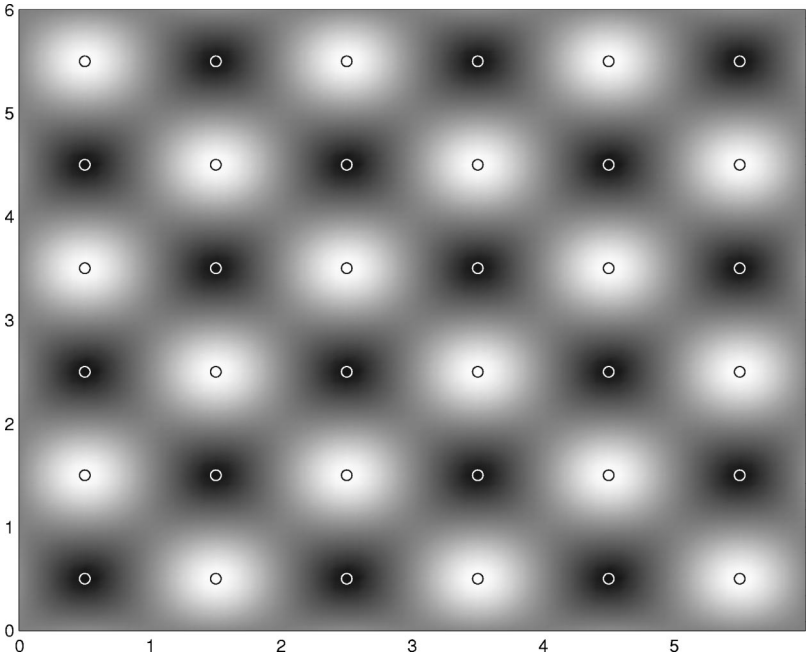

FIG. 2. Simulated STM image of $Ni_3Al(001)$ surface received in constant-height mode. Tip-sample distance equals to 5.23 Å. Black and white circles denote the positions of Al and Ni surface atoms, respectively. Coordinates are expressed in the units of the nearest-neighbor distance (2.49 Å).

$$\hat{H}^{mb} = \sum_i U_i \hat{n}_{i,\uparrow} \hat{n}_{i,\downarrow} + \frac{1}{2} \sum_{i,j \neq i,\delta} (J_{ij} \hat{n}_{i\delta} \hat{n}_{j\delta'} + \tilde{J}_{ij} \hat{n}_{i\delta} \hat{n}_{j\delta}). \tag{10}$$

In Eq. (9), $E_{i\delta}$ represent the different orbital levels and $T_{ij,\delta}$ denote their hopping interactions, while U_i, J_{ij}, and $\tilde{J}_{ij}$ in Eq. (10) are the intrasite and intersite Coulomb interactions between orbitals *i* and *j*, respectively. Their values have been obtained by using the wave functions of the independent atoms forming the system (for more details, see Refs. 14 and 15). The many-body contributions are treated within our LCAO formulation by using an extension of the local-denisty approximation.[14] It enables us to include these contributions introducing the Hartree and exchange-correlation potentials for each orbital, taking into account its occupancy and the corresponding intrasite and intersite interactions, appearing in Eqs. (8)–(10).[14] Using these many-body potentials the LCAO Hamiltonian can be solved self-consistently, which allows us to find the occupancy of different orbitals at different atoms, and as a result obtain the distribution of the electronic charge in the whole system.

This method has been earlier applied to a successful calculation of the chemisorption energy and the charge transfer of Na/Al(001), Cl/GaAs, K/GaAs, and a number of other systems (see, e.g., Refs. 14 and 16–18). It has also been used for theoretical studies of the passivation process of semiconductor surfaces,[14,19] and the adsorption of rare gases on metal surfaces.[12] In the present paper, we have used this approach to obtain the matrices of Green functions and density of states of Ni_3Al surfaces, which are necessary to compute the tunneling current [cf. Eq. (4)].

On the other hand, the matrices of Green functions and density of states of the tip, which are also needed in Eq. (4), have been calculated with the help of the cluster-Bethe-lattice method.[20] In the framework of this approach we have assumed that the topmost part of this tip is represented by a pyramidal cluster of five atoms: one atom at the apex and four at the base of this pyramid. Each atom of this base is then joined to a Bethe-lattice that simulates the influence of the rest of the tip. It means that the electronic properties of this system have been calculated by projecting each Bethe lattice onto the atom of the pyramid to which it is joined. This allows us to calculate the density of states and Green-function matrices by solving the reduced system formed by the atoms of the pyramid located around the tip apex. Electronic structure of the apex part of the tip is then determined by properties of this topmost apex due to its geometry modified by the rest of the tip simulated by Bethe lattice. We have introduced a self-consistency by imposing a local charge neutrality condition at each atom of this topmpost cluster.

It should be pointed out that the calculations presented in this paper have been performed with the assumption that the atomic structure of (111) and (001) surfaces is ideal, i.e., all distances between atoms in the surface regions are the same as in the bulk. It means that we are neglecting in STM simulations the small vertical displacement of surface Al atoms with respect to the Ni atoms [0.02 Å and 0.06 Å for (001) and (111) surfaces, respectively[2,3]].

IV. RESULTS OF STM SIMULATIONS

Figures 2 and 3 present the calculated STM images of the (001) and (111) surfaces, respectively. In general, we can say that the theoretical results confirm the STM measurements of $Ni_3Al(111)$ (see Fig. 1) and their interpretation given in Ref. 4: The simulated images show the 2×2 surface superstructure built up only by Al atoms and the lack of Ni surface atoms. Black small circles in Figs. 2 and 3 denote the positions of surface Al atoms while white circles correspond to Ni atoms.

The STM simulations have been performed for a tungsten tip and in the constant-height mode with a tip-surface dis-

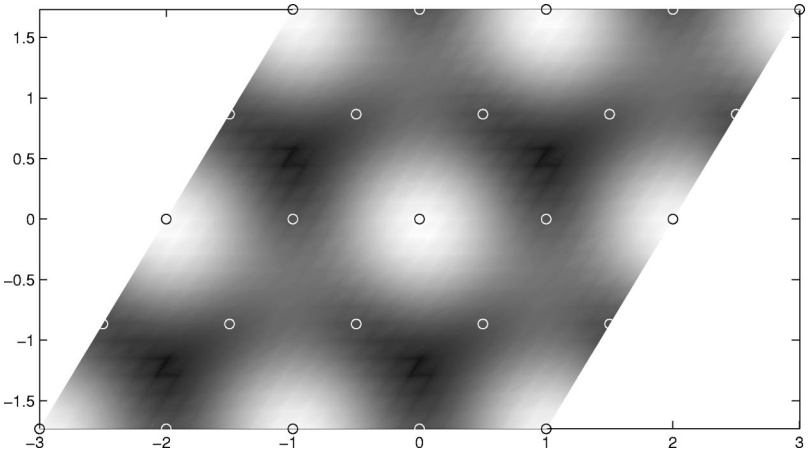

FIG. 3. The same as in Fig. 2, but for $Ni_3Al(111)$ surface.

tance of 5.23 Å. Both images present the changes of the conductance along the Ni_3Al surfaces; it means that their topographies were built up only by tunneling through the states from the Fermi levels of the tip and the substrate (zero voltage limit). This assumption corresponds well with the conditions of the STM measurements, which were performed for very small voltages (20 mV).

The density-of-states distributions at the (001) and (111) surfaces are shown in Figs. 4 and 5, respectively. For the considered conditions (tip-surface separation equals to 5.23 Å) the most important current contributions are connected with s and p_z states of the surface atoms (p_z is oriented perpendicular to the surface) and therefore only the energy distributions of these states are presented in Figs. 4 and 5. In the case of the (111) surface (see Fig. 5) we can notice that near the Fermi level the density of s and p_z states at Al atoms is higher than at Ni atoms, which might be partially responsible for the domination of Al atoms in Fig. 3. But this argument does not work in the case of the (001) surface (see Fig. 2), where the densities of s and p_z states at the Fermi level are almost the same at Al and Ni atoms (see Fig. 4), and therefore this factor cannot be a reason for the large differences between the current contributions flowing through these atoms.

In our theoretical study we wanted to clarify the role of the interorbital interference in the STM tunneling process and its possible influence on the topographies in STM images. We should note that the general expression for the tunneling current, which has been used in our STM simulations [cf. Eq. (4)], involves taking the trace of a multiplication of several matrices. This can physically be interpreted as a coherent superposition of different channels formed by different orbitals of the atoms from the tip and the substrate surface. Therefore, this multichannel approach allows us to consider the effects connected with interference of the tunneling through different orbitals of the tip-substrate system.

A detailed study of the tunneling through different orbitals of the surface atoms leads to the conclusion that the strong difference between the current components flowing through Al and Ni surface atoms is caused to large extent by the interference of the tunneling through s and p_z orbitals of these atoms. This effect can be illustrated by the analysis of the different contributions to the whole tunneling current. Figure 6 presents the conductance for the tip moving over the surface along a dense-packed row of Al and Ni atoms of the (001) surface. This figure shows the changes of the total conductance (solid line) and different contributions for tunneling through different orbitals of the $Ni_3Al(001)$ substrate. For larger tip-sample separations the current contributions connected with d orbitals of the substrate are not playing an important role (in the considered case the d orbitals contrib-

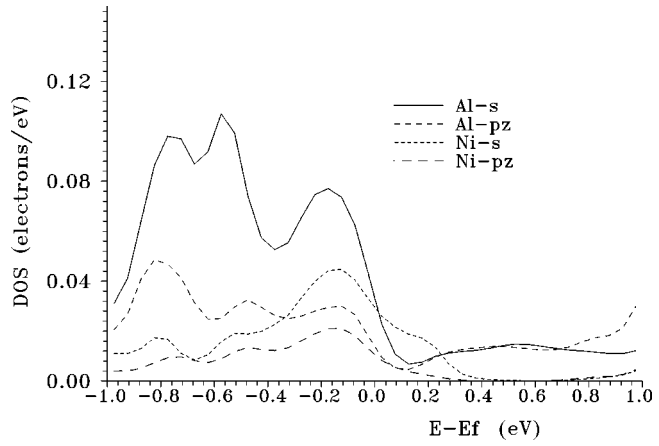

FIG. 4. Distributions of s and p_z states of surface Al and Ni atoms at $Ni_3Al(001)$ (see legend).

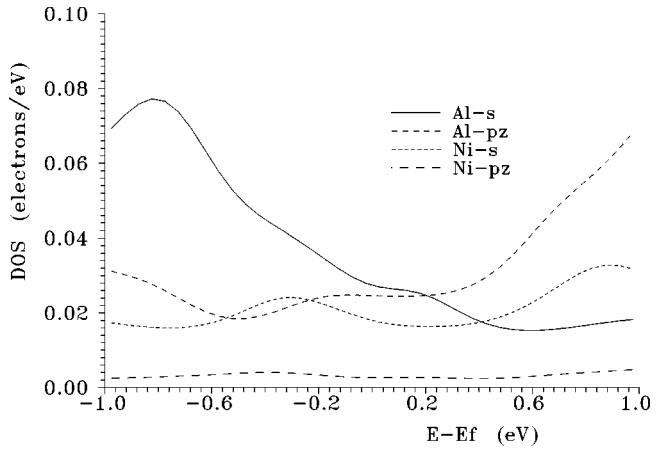

FIG. 5. The same as in Fig. 2, but for $Ni_3Al(111)$ surface.

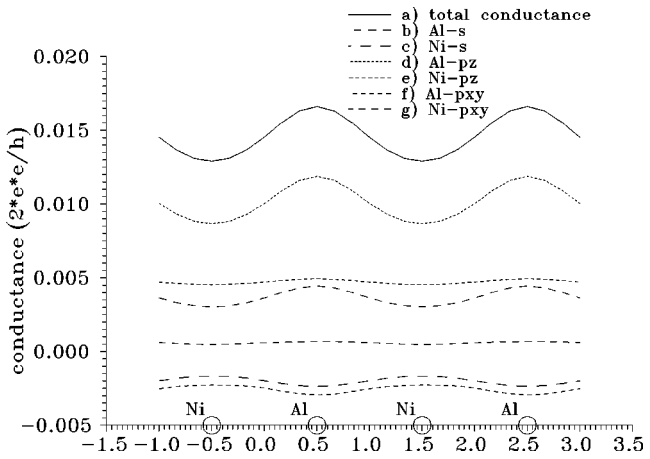

FIG. 6. Variation of the conductance for the tip moving along a dense-packed row of Al and Ni atoms of the $Ni_3Al(001)$ surface, under tunneling conditions as in Fig. 2: Total conductance (solid line), as well as the s, p_z, and p_{xy} contributions connected with the tunneling through surface Al and Ni atoms (see legend). Values along the horizontal axis are expressed in the units of the nearest-neighbor distance (2.49 Å).

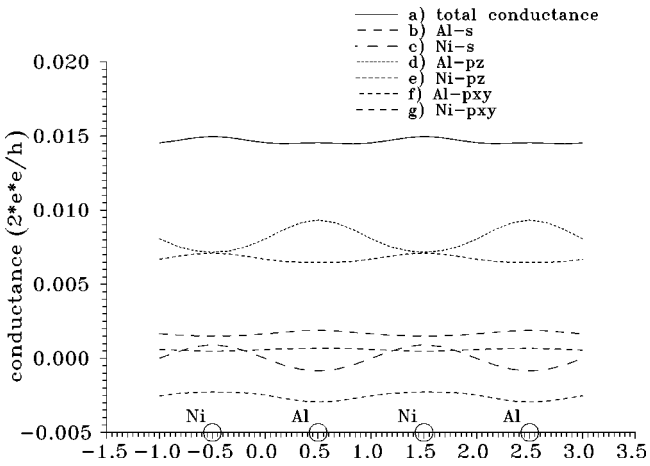

FIG. 7. The same as in Fig. 6, but without the intra-atomic s-p_z interference.

ute only by a few percent to the whole tunneling current), and therefore Fig. 6 presents only the variation of s and p_z current components corresponding to Ni and Al surface atoms.

It follows from the presented dependences that the topography in STM images is built up mainly by the tunneling through s and p_z orbitals of Al atoms: these current contributions have sharp maxima above Al atoms, which influence the variation of the whole tunneling current significantly. As a result, only Al surface atoms are visible in simulated STM images (see Fig. 2). Figure 6 also shows the important differences between the current contributions connected with s and p_z orbitals of Ni and Al atoms. The density-of-states distribution presented in Fig. 4 shows that near the Fermi level the density of p_z states at Al atoms is only about 20% higher than at Ni atoms, but their contributions to the tunneling process are very different. The p_z orbitals of Al and Ni atoms are oriented perpendicular to the alloy surface, but only the variation of the Al-p_z current component seems to reproduce the localization properties of these orbitals (the Al-p_z contribution has strong maxima above Al atoms). The Ni-p_z current component has an almost flat characteristic along the surface with small maxima above Al atoms; of course, this effect cannot be explained by the localization properties of Ni-p_z orbitals.

The densities of s states at Ni and Al atoms are almost the same near the Fermi level (see Fig. 4), but the variation of their current components is also drastically different. In the case of Al atoms, the s contributions increase considerably the current flowing through these atoms, while in the case of Ni atoms the s component has a negative sign and reduces the current tunneling through Ni atoms. As a consequence, the current flowing through Ni atoms is much lower than it follows from the proportion of the densities of states at Ni and Al atoms. The investigation of the STM process based only on the analysis of the density of states at particular surface atoms and the localization properties of the orbitals involved in the tunneling is obviously insufficient in this case.

In order to clarify the role of the of interorbital interference in the tunneling of electrons in the considered system, we have repeated the simulation removing selectively these off-diagonal elements from the Green functions and the density of states matrices, which are responsible for the interatomic and intra-atomic interorbital interference in the tunneling process. The detailed analysis leads to the conclusion that the domination of Al atoms in the STM images of Ni_3Al is caused to a large degree by the intra-atomic interference of the tunneling through s and p_z orbitals in Al and Ni atoms. Figure 7 shows the STM profile (as in Fig. 6), calculated for the case when s-p_z intra-atomic elements were removed from the matrices of the Green functions and the densities of states of Ni_3Al. As it follows from these dependences (see Fig. 7), the variation of the total current now looks completely different. The comparison between Figs. 6 and 7 clearly shows that the removal of intra-atomic s-p_z interference reduces considerably the s and p_z contributions flowing through Al atoms (it reduces their averaged values and also their relative variation along the surface). On the other hand, the s and p_z contributions tunneling through Ni atoms are increased and now they reproduce very well the localization of particular Ni atoms (compare Ni-s and Ni-p_z contributions in Figs. 6 and 7). As a consequence, the relative variation of the total tunneling current along the surface is now around 90% smaller. Flat maxima appear now above Ni atoms and also (but smaller ones) above Al atoms (the corresponding two-dimensional picture is shown in Fig. 8).

The detailed study shows that the intra-atomic s-p_z interference has the most significant influence on the variation of the tunneling current. In Fig. 9 we can see the comparison between the STM profiles calculated with the complete Green functions and densities of states matrices (solid line), without interatomic interactions, without s-p_z intra-atomic interactions, and without all off-diagonal (intra-atomic and interatomic) elements. It follows from this sequence that the most drastic change of the scanline is caused by the removal of the s-p_z intra-atomic interactions, while in this case, the

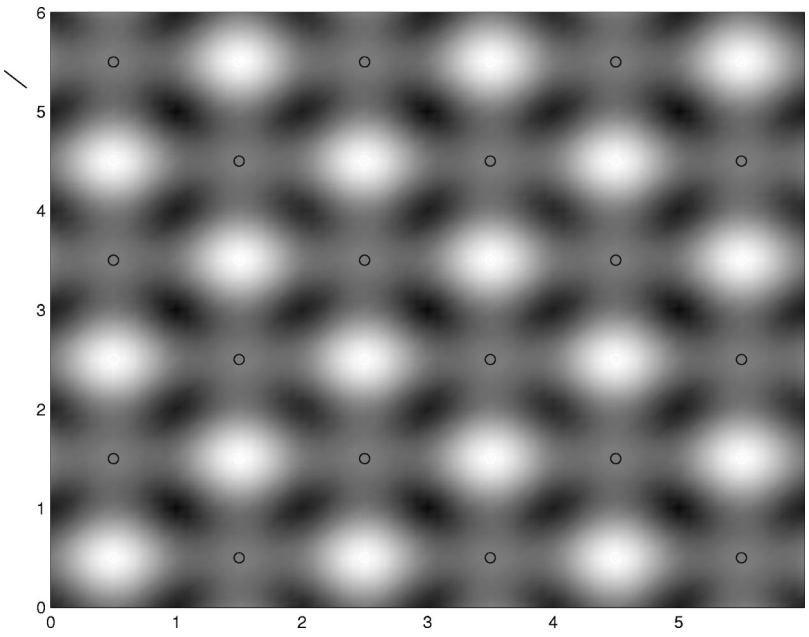

FIG. 8. The same as in Fig. 2, but without the intra-atomic s-p_z interference.

interatomic effects do not influence the variation of the total tunneling current significantly.

These results show that in the case of the Ni surface atoms the intra-atomic s-p_z interference reduces the value of the s and p_z contributions and their variations along the surface, while in the case of Al atoms the same mechanism leads to the opposite result: The value and the changes of s and p_z current contributions increase considerably and, as a consequence, the STM images of $Ni_3Al(001)$ show only Al atoms. It means that the intra-atomic s-p_z interference may either have destructive influence on s and p_z current contributions (reducing their values and variations) or may increase the efficiency of tunneling through these orbitals. Additional studies show that this effect depends in general on the energy of the states, which are active in the tunneling, with respect to the potentials of the s and p_z orbitals, i.e., E_s and E_{p_z}, respectively (one-center integrals in the LCAO language). When the tunneling takes place through the states with energies significantly lower than E_s and E_{p_z}, then the intra-atomic s-p_z interference reduces the effectivity of the tunneling through s and p_z orbitals. On the other hand, for tunneling from the energy range between E_s and E_{p_z}, the intra-atomic s-p_z interference increases considerably the s and p_z current components. In the STM simulations performed for Ni_3Al, the electronic states of the alloy, which are active in the tunneling, are located very close to the Fermi level E_f, lying deep below E_s and E_{p_z} of the Ni atoms, but between E_s and E_{p_z} of Al atoms. As a result, the intra-atomic s-p_z interference reduces the current flowing through s and p_z orbitals of Ni atoms and increases the respective contributions tunneling through Al surface atoms. The above results of STM simulations indicate that this mechanism is responsible for the domination of Al atoms in the STM image of $Ni_3Al(001)$.

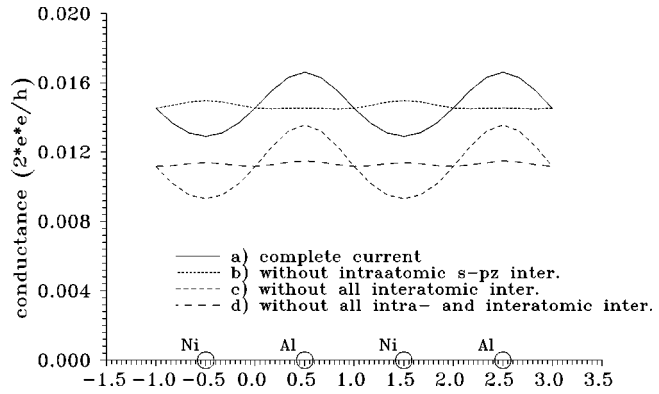

FIG. 9. The comparison of STM profiles along $Ni_3Al(001)$ (as in Figs. 7 and 8), calculated with different modifications of the Green functions and the density of states matrices.

It was mentioned above that in the case of the (001) surface the interatomic effects do not influence the variation of

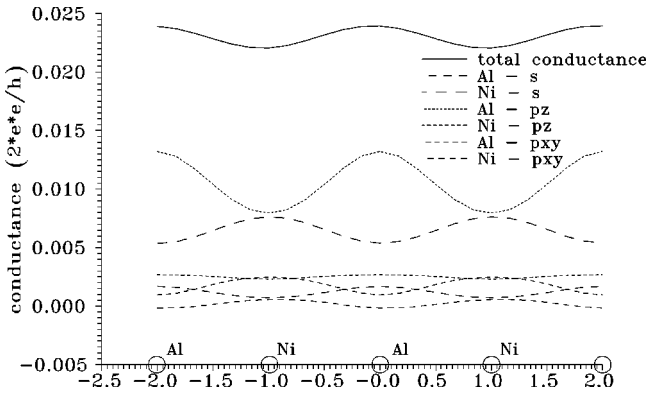

FIG. 10. Variation of the conductance for the tip moving along a dense-packed row of Al and Ni atoms of the $Ni_3Al(111)$ surface, under tunneling conditions as in Fig. 3: Total conductance (solid line), as well as the s, p_z, and p_{xy} contributions connected with the tunneling through surface Al and Ni atoms (see legend). Values along the horizontal axis are expressed in units of the nearest-neighbor distance (2.49 Å).

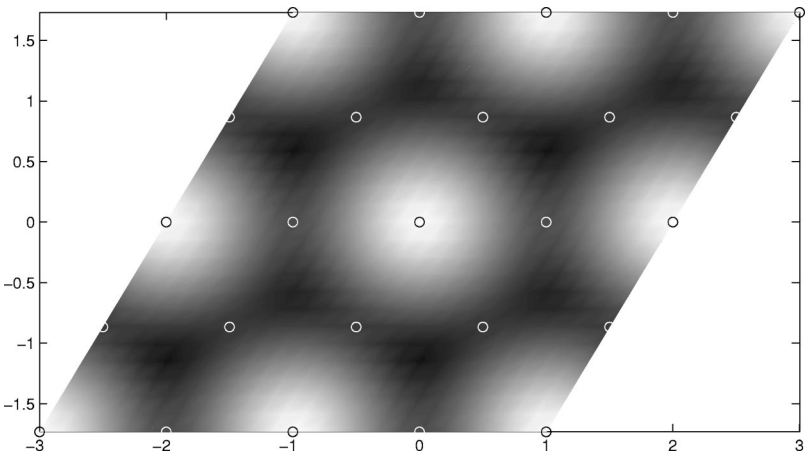

FIG. 11. The same as in Fig. 3, but without the interatomic interference.

the tunneling current significantly (compare curves *a* and *c* in Fig. 9), and in this case the key role in the formation of STM images is mainly due to the intra-atomic s-p_z interference. As surface atoms at (111) surfaces are more dense packed than at (001), we might expect that in this case the interatomic effects play a more important role.

The results obtained for the (111) surface (see Figs. 3 and 10) indicate that like before [i.e., for (001) surface], the dominating current contributions flow through surface Al atoms (mainly through their p_z orbitals) and thus only these atoms are visible in the simulated STM images. On the other hand, these results show that in the case of the (111) surface the interatomic effects modify the tunneling current much stronger as compared to (001) surfaces. We can note that now the interatomic interference strongly increases the value of the total conductance and reduces considerably its variation along the surface. As a result, the simulated image of the $Ni_3Al(111)$ surface is more flat than in the case of the (001) surface. The variation of the total conductance along the (001) and (111) surfaces is equal to 30% and 9%, respectively (compare Figs. 6 and 10). The obtained results also show that for (111) surfaces the interatomic interference modifies the topography of the STM image significantly. Besides the superstructure formed by the Al atoms, we can notice in Fig. 3 the trianglelike dark regions located between surface Al atoms (these features are also well visible in STM images detected in the experiment; cf. Fig. 1). The comparison of Fig. 3 with Fig. 11 [which is the STM image of $Ni_3Al(111)$ calculated without interatomic effects] clearly shows that the appearance of these trianglelike features is caused by the interatomic interference. The localization of such dark triangular regions is correlated with the structure of the lower atomic plane in such a way that the center of each triangle is located directly above an Al atom in the second layer. It indicates that the appearance of these trianglelike features in STM images are caused by the influence of deeper atomic layers.

The results presented in Fig. 12 show also that, like for the (001) surface, the domination of Al atoms in STM images is caused to a large degree by s-p_z intereference. However, contrary to the (001) surface, this effect for the (111) surface is also supported by the higher densities of s and p_z states at Al surface atoms (cf. Fig. 5). The intra-atomic s-p_z interference influences the tunneling current in the same way as for the (001) surface, i.e., it increases the current flowing through s and p_z orbitals of Al atoms and reduces the respective current contributions connected with Ni atoms. The comparison between curves *a* and *b* of Fig. 12 shows that this interaction contributes significantly to the appearance of the Al superstructures in the STM images (the removal of intra-atomic s-p_z interference leads to a virtually flat shape of the STM profile; cf. curve *b* in Fig. 12).

As it has already been mentioned, both Ni_3Al surfaces are assumed to be flat in our considerations, i.e., we neglect the small vertical displacements of surface atoms. As follows from other calculations,[2,3] Al atoms are shifted up with respect to Ni atoms by 0.02 Å and 0.06 Å at (001) and (111) surfaces, respectively. This has not been taken into account in our study. In the case of the (001) surface, the displacement of Al and Ni atoms is so small that it virtually does not influence the STM process, hence our assumption of this surface to be flat seems to be well justified. The simulations performed for (111) surface—again assuming that Al and Ni surface atoms are located at the same level—also give the topography of STM image corresponding very well to experimental results, as discussed above. However, the additional calculations performed in a constant-current mode show that the height of STM corrugation computed for the (111) surface is two times smaller than the measured value

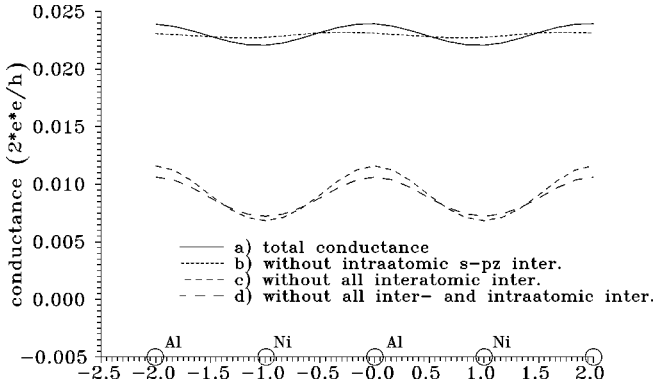

FIG. 12. The comparison of STM profiles along $Ni_3Al(111)$ (as in Fig. 10), calculated with different modifications of the Green functions and density of states matrices.

(which is 18 pm, as seen in Fig. 1). This discrepancy might be due to the displacement of surface Al and Ni atoms, neglected in our calculations. Since at the (111) surface this displacement is three times greater than at the (001) surface, it might indeed provide, apart from the intra-atomic s-p_z interference, an additional contribution resulting in the domination of Al atoms in the STM image of the (111) Ni_3Al surface. Consequently, this issue merits further theoretical considerations.

V. CONCLUSIONS

The results of STM simulations presented are best fit to STM measurements performed for $Ni_3Al(111)$ surfaces. The topographies of the images obtained from the experiment and the numerical computations are the same and present a superstructure formed by surface Al atoms, while Ni atoms remain invisible.

Our theoretical study indicates clearly that the tunneling process at (001) and (111) surfaces is strongly influenced by the intra-atomic s-p_z interference. This kind of intra-atomic interference reduces s and p_z current contributions flowing through Ni atoms, but on the other hand it increases considerably s and p_z contributions connected with surface Al atoms. A detailed analysis has shown that this is the crucial factor responsible for the domination of Al surface atoms in the STM images of the Ni_3Al (001) surface, and it also plays an important role in the formation of the image of the (111) surface. Theoretical investigations presented in this paper also enabled us to explain the appearance of trianglelike features as a result of the influence of the subsurface atomic layer.

The influence of the intra-atomic s-p_z interference on the formation of STM images represents the general and important problem. This factor causes the differences between the height and type of STM corrugation seen at different metal surfaces. In particular, it is responsible, at least partially, for the unexpectedly high corrugation of some metal surfaces, as indicated by STM measurements, which cannot be explained simply by the charge distribution along the substrate surface.

ACKNOWLEDGMENT

One of the authors (L.J.) thanks University of Wrocław for support within the Grant No. 2016/W/IFD/02.

[1] D. Sondericker, F. Jona, V.L. Moruzzi, and P.M. Marcus, Solid State Commun. **53**, 175 (1985).
[2] D. Sondericker, F. Jona, and P.M. Marcus, Phys. Rev. B **33**, 900 (1986).
[3] D. Sondericker, F. Jona and P.M. Marcus, Phys. Rev. B **34**, 6770 (1986).
[4] A. Rosenhahn, J. Schneider, C. Becker, and K. Wandelt, Appl. Surf. Sci. **142**, 169 (1999).
[5] M. Schmidt, M. Nohlen, G. Bermes, and K. Wandelt, Rev. Sci. Instrum. **68**, 3866 (1997).
[6] M. Wilms, M. Schmidt, G. Bermes, and K. Wandelt, Rev. Sci. Instrum. **69**, 2696 (1998).
[7] L.V. Keldysh, Zh. Éksp. Teor. Phys. **47**, 1515 (1964) [Sov. Phys. JETP **20**, 1018 (1965)].
[8] C. Caroli, R. Combescot, P. Nozières, and D. Saint-James, J. Phys. C **4**, 916 (1971).
[9] C. Caroli, R. Combescot, P. Nozières, and D. Saint-James, J. Phys. C **5**, 21 (1972).
[10] A. Martin-Rodero, F. Flores, and N.H. March, Phys. Rev. B **38**, 10 047 (1988).
[11] J. Ferrer, A. Martin-Rodero, and F. Flores, Phys. Rev. B **38**, 10 113 (1988).
[12] N. Mingo, L. Jurczyszyn, F.J. Garcia-Vidal, R. Saiz-Pardo, P.L. de Andres, F. Flores, S.Y. Wu, and W. More, Phys. Rev. B **54**, 2225 (1996).
[13] E.C. Goldberg, A. Martin-Rodero, R. Monreal, and F. Flores, Phys. Rev. B **39**, 5684 (1989).
[14] F.J. Garcia-Vidal, J. Merino, R. Perez, R. Rincon, J. Ortega, and F. Flores, Phys. Rev. B **50**, 10 537 (1994).
[15] F.J. Garcia-Vidal, A. Martin-Rodero, F. Flores, J. Ortega, and R. Perez, Phys. Rev. B **44**, 11 412 (1991).
[16] F. Flores, R. Rincon, and F.J. Garcia-Vidal, Appl. Surf. Sci. **92**, 216 (1996).
[17] R. Saiz-Pardo, R. Rincon, and F. Flores, Appl. Surf. Sci. **92**, 362 (1996).
[18] F. Flores, A. Levy Yevati, A. Martin-Rodero, J. Ortega, and R. Rincon, Appl. Surf. Sci. **104-105**, 248 (1996).
[19] F. Flores, R. Saiz-Pardo, R. Rincon, and P.L. De Andres, Appl. Surf. Sci. **104-105**, 183 (1996).
[20] L. Martin-Moreno and J.A. Verges, Phys. Rev. B **42**, 7193 (1990).